Ground-state phases of ultracold bosons with Rashba-Dresselhaus spin-orbit coupling

Tomoki Ozawa and Gordon Baym

Phys. Rev. A **85**, 013612 — Published 9 January 2012

DOI: 10.1103/PhysRevA.85.013612

Ground state phases of ultracold bosons with Rashba-Dresselhaus spin-orbit coupling

Tomoki Ozawa and Gordon Baym
Department of Physics, University of Illinois at Urbana-Champaign, 1110 W. Green St., Urbana, Illinois 61801, USA

We study ultracold bosons in three dimensions with an anisotropic Rashba-Dresselhaus spin-orbit coupling. We first carry out the exact summation of ladder diagrams for the two boson t-matrix at zero energy. Then, with the t-matrix as the effective interaction, we find the ground state phase diagrams of bosons in mean field, as a function of the spin-orbit coupling, the anisotropy, and the scattering lengths between particles in the same and in different pseudospin states. The resulting phase diagrams have a much richer structures than those obtained using mean-field couplings, exhibiting three different phases: a plane wave condensate, a striped condensate, and an unstable phase. The differences between the present approach using the t-matrix compared using mean-field couplings is significant for large scattering lengths, large spin-orbit coupling strength, or small anisotropy.

I. INTRODUCTION

Spin-orbit coupling plays a crucial role in a variety of physical systems ranging from atoms and nuclei to topological insulators [1] and spintronics [2]. Recently, the prospect of realizing spin-orbit coupling in ultracold atomic systems has led to increased interest not only in fermions but also bosons for this purpose [3]. Currently proposed and realized schemes to produce spin-orbit coupling in ultracold atomic systems create effective non-Abelian gauge fields for atoms [3–9] which take the form of Rashba-Dresselhaus spin-orbit couplings, familiar in semiconductor physics [10, 11]. A system of spin-orbit coupled ultracold bosons was recently realized by Lin et al. [4].

The problem of ultracold bosons with Rashba-Dresselhaus spin-orbit coupling has been considered within mean-field, where the interparticle interactions are assumed to be independent of momenta [12–17]. These studies predicted that the ground states can be either a "plane wave" Bose-Einstein condensate (BEC) of particles in a single momentum state, or a "striped" BEC involving a coherent superposition of two different momenta. However, recent studies indicate that beyond mean-field the effective interaction has a qualitatively different structure, resulting, e.g., in the absence of interaction between particles scattering in the zero total-momentum channel [18, 19], and the prediction that a BEC involving only a single momentum of particles is not favorable in an isotropic Rashba field [18].

In this study we delineate the ground state phase diagram of bosons taking the effective interaction described in terms of the full t-matrix rather than mean-field coupling. We consider bosons with an isotropic or anisotropic Rashba-Dresselhaus spin-orbit coupling, $\sim \kappa(\sigma_x p_x + \eta\sigma_y p_y)$, where κ is the spin-orbit coupling strength, $\mathbf{p}$ is the particle momentum, and η determines the x-y anisotropy. In our previous paper [19], we showed that the effective interaction can be renormalized in terms of physical scattering lengths and does not depend on the ultraviolet cutoffs. Here we extend this calculation, and carry out the exact summation of ladder diagrams for the t-matrix of bosons scattering at zero energy, in three dimensions. Then we reduce the Hamiltonian, with the t-matrix as the effective interaction, to a Nozières model [20], from which we determine the ground state phases as functions of the anisotropies in the κa_{aa}-κa_{ab} plane, where a_{aa} and a_{ab} are the scattering lengths between the same and different pseudospin states, respectively. We show that there are generally three phases: a plane wave BEC, a striped BEC with two different momenta, and an unstable phase where the effective interaction is attractive [25]. The phase diagrams (Figs. 2 and 3 below) are substantially different and richer in structure than those predicted using mean-field couplings with the bare couplings replaced by $4\pi\hbar^2 a_{ij}/m$, especially when κa_{aa} and κa_{ab} are large, or η is close to unity. In the isotropic limit $\eta = 1$, the plane wave BEC does not appear (Fig. 3). We describe how the phase diagram evolves continuously with anisotropy, from $\eta = 0$ where spin-orbit coupling is present only in the x-direction, to an isotropic spin-orbit coupling $\eta = 1$. We find that in the vicinity of $\eta = 1$, the phase diagrams are logarithmically sensitive to small changes in η, a structure we analyze by expanding in the anisotropy about $\eta = 1$. We also find that a BEC with negative scattering lengths can be stabilized in the presence of spin-orbit coupling, when the scattering lengths are sufficiently large in magnitude (Fig. 4).

Our analysis can be directly compared with proposed experimental schemes [5–9] when the scattering lengths are all equal, a good approximation for the three $F = 1$ hyperfine states of ^{87}Rb. We discuss in this situation how the phases of bosons in the ground state evolve with varying anisotropy and scattering length (Fig. 5). In the following we take $\hbar = 1$.

II. HAMILTONIAN

We consider bosons in three dimensions with a Rashba-Dresselhaus spin-orbit coupling, described by the Hamiltonian

$$\mathcal{H} = \sum_{\mathbf{p}} \left(a^\dagger_{\mathbf{p}} \;\; b^\dagger_{\mathbf{p}}\right) \left[\frac{p^2+\kappa^2}{2m} I + \frac{\kappa}{m}(\sigma_x p_x + \eta \sigma_y p_y)\right] \begin{pmatrix} a_{\mathbf{p}} \\ b_{\mathbf{p}} \end{pmatrix} + \frac{1}{2V} \sum_{\mathbf{p}_1+\mathbf{p}_2=\mathbf{p}_3+\mathbf{p}_4} \left(g_{aa} a^\dagger_{\mathbf{p}_4} a^\dagger_{\mathbf{p}_3} a_{\mathbf{p}_2} a_{\mathbf{p}_1} + g_{bb} b^\dagger_{\mathbf{p}_4} b^\dagger_{\mathbf{p}_3} b_{\mathbf{p}_2} b_{\mathbf{p}_1} + 2 g_{ab}\; a^\dagger_{\mathbf{p}_4} b^\dagger_{\mathbf{p}_3} b_{\mathbf{p}_2} a_{\mathbf{p}_1}\right). \quad (1)$$

As in our previous paper [19], m is the atomic mass, V is the volume of the system, $a_{\mathbf{p}}$ annihilates an atom the pseudospin state a with momentum $\mathbf{p}$, and $b_{\mathbf{p}}$ annihilates an atom in pseudospin state b with momentum $\mathbf{p}$; the σ_x and σ_y are the usual Pauli matrices between the internal states, and I is the two-by-two identity matrix. We take the coupling κ to be positive. The g_{aa}, g_{bb}, and g_{ab} are the bare s-wave couplings between a-a, b-b, and a-b particles. When the system is isotropic, $\eta = 1$, the Hamiltonian completely reduces to that considered previously [19]. In practice the effective Hamiltonian, in the basis in which the coupling has the Rashba-Dresselhaus form, can contain terms that do not conserve the individual number of particle of each species (a-like and b-like); we ignore such terms at this point, and return to this issue below.

To diagonalize the single particle part of the Hamiltonian we introduce operators $\alpha_{\mathbf{p}}$ and $\beta_{\mathbf{p}}$ defined by

$$\begin{pmatrix} \alpha_{\mathbf{p}} \\ \beta_{\mathbf{p}} \end{pmatrix} = \frac{1}{\sqrt{2}} \begin{pmatrix} 1 & -e^{-i\phi} \\ 1 & e^{-i\phi} \end{pmatrix} \begin{pmatrix} a_{\mathbf{p}} \\ b_{\mathbf{p}} \end{pmatrix}, \quad (2)$$

where ϕ is the angle of $(p_x, \eta p_y)$ in the x-y plane. Note that for a given momentum ϕ depends on η. In terms of the α's and β's the Hamiltonian becomes

$$\mathcal{H} = \sum_{\mathbf{p}} \left(\epsilon_-(\mathbf{p}) \alpha^\dagger_{\mathbf{p}} \alpha_{\mathbf{p}} + \epsilon_+(\mathbf{p}) \beta^\dagger_{\mathbf{p}} \beta_{\mathbf{p}}\right) + \mathcal{H}_{\rm int}. \quad (3)$$

The single-particle spectrum has two branches

$$\epsilon_\pm(\mathbf{p}) = \frac{1}{2m}\left[\left(\sqrt{p_x^2 + \eta^2 p_y^2} \pm \kappa\right)^2 + (1-\eta^2) p_y^2 + p_z^2\right]; \quad (4)$$

the single particle ground state is given by the lower branch $\epsilon_-(\mathbf{p})$, which has degenerate states on the circle $\sqrt{p_x^2 + p_y^2} = \kappa$ and $p_z = 0$ when $\eta = 1$, and two-fold degeneracy for $\mathbf{p} = (\pm\kappa, 0, 0)$ when $0 \le \eta < 1$.

The interaction part $\mathcal{H}_{\rm int}$ is as in Ref. [19], except for the η dependence:

$$\begin{aligned} \mathcal{H}_{\rm int} = \frac{1}{V} \sum_{\mathbf{p}_1+\mathbf{p}_2=\mathbf{p}_3+\mathbf{p}_4} & \Big[\mathcal{V}^{(1)}_{\phi_1,\phi_2;\phi_3,\phi_4} \left(\alpha^\dagger_{\mathbf{p}_4}\alpha^\dagger_{\mathbf{p}_3}\alpha_{\mathbf{p}_2}\alpha_{\mathbf{p}_1} + \beta^\dagger_{\mathbf{p}_4}\beta^\dagger_{\mathbf{p}_3}\beta_{\mathbf{p}_2}\beta_{\mathbf{p}_1}\right)/2 \\ & + \mathcal{V}^{(2)}_{\phi_1,\phi_2;\phi_3,\phi_4} \left(\beta^\dagger_{\mathbf{p}_4}\beta^\dagger_{\mathbf{p}_3}\alpha_{\mathbf{p}_2}\alpha_{\mathbf{p}_1} + \alpha^\dagger_{\mathbf{p}_4}\alpha^\dagger_{\mathbf{p}_3}\beta_{\mathbf{p}_2}\beta_{\mathbf{p}_1}\right)/2 \\ & + \mathcal{V}^{(3)}_{\phi_1,\phi_2;\phi_3,\phi_4} \left(\alpha^\dagger_{\mathbf{p}_4}\beta^\dagger_{\mathbf{p}_3}\beta_{\mathbf{p}_2}\beta_{\mathbf{p}_1} + \beta^\dagger_{\mathbf{p}_4}\alpha^\dagger_{\mathbf{p}_3}\alpha_{\mathbf{p}_2}\alpha_{\mathbf{p}_1}\right)/\sqrt{2} \\ & + \mathcal{V}^{(4)}_{\phi_1,\phi_2;\phi_3,\phi_4} \left(\alpha^\dagger_{\mathbf{p}_4}\alpha^\dagger_{\mathbf{p}_3}\beta_{\mathbf{p}_2}\alpha_{\mathbf{p}_1} + \beta^\dagger_{\mathbf{p}_4}\beta^\dagger_{\mathbf{p}_3}\alpha_{\mathbf{p}_2}\beta_{\mathbf{p}_1}\right)/\sqrt{2} \\ & + \mathcal{V}^{(5)}_{\phi_1,\phi_2;\phi_3,\phi_4} \alpha^\dagger_{\mathbf{p}_4}\beta^\dagger_{\mathbf{p}_3}\beta_{\mathbf{p}_2}\alpha_{\mathbf{p}_1}\Big], \end{aligned} \quad (5)$$

where ϕ_i is the angle of $(p_{i,x}, \eta p_{i,y})$ in the x-y plane, dependent on η, and the $\mathcal{V}^{(i)}$'s are

$$\begin{aligned} \mathcal{V}^{(1)}_{\phi_1,\phi_2;\phi_3,\phi_4} &= A_+ + \frac{g_{ab}}{8}\left(e^{i\phi_1} + e^{i\phi_2}\right)\left(e^{-i\phi_3} + e^{-i\phi_4}\right) \\ \mathcal{V}^{(2)}_{\phi_1,\phi_2;\phi_3,\phi_4} &= A_+ - \frac{g_{ab}}{8}\left(e^{i\phi_1} + e^{i\phi_2}\right)\left(e^{-i\phi_3} + e^{-i\phi_4}\right) \\ \mathcal{V}^{(3)}_{\phi_1,\phi_2;\phi_3,\phi_4} &= \sqrt{2}A_- + \frac{g_{ab}}{4\sqrt{2}}\left(e^{i\phi_1} + e^{i\phi_2}\right)\left(e^{-i\phi_3} - e^{-i\phi_4}\right) \\ \mathcal{V}^{(4)}_{\phi_1,\phi_2;\phi_3,\phi_4} &= \sqrt{2}A_- + \frac{g_{ab}}{4\sqrt{2}}\left(e^{i\phi_1} - e^{i\phi_2}\right)\left(e^{-i\phi_3} + e^{-i\phi_4}\right) \\ \mathcal{V}^{(5)}_{\phi_1,\phi_2;\phi_3,\phi_4} &= 2A_+ - \frac{g_{ab}}{4}\left(e^{i\phi_1} - e^{i\phi_2}\right)\left(e^{-i\phi_3} - e^{-i\phi_4}\right), \end{aligned} \quad (6)$$

with

$$A_\pm = \left(g_{aa} \pm g_{bb} e^{i(\phi_1+\phi_2-\phi_3-\phi_4)}\right)/4. \quad (7)$$

III. THE T-MATRIX

We now turn to calculating the scattering t-matrix, $\Gamma^{\alpha\alpha}_{\alpha\alpha}(\mathbf{p}, \mathbf{p}'; \mathbf{q})$, for two bosons in the ground states of the lower (α) branch, with incoming momenta $\mathbf{q}/2 + \mathbf{p}$ and $\mathbf{q}/2 - \mathbf{p}$, and outgoing momenta $\mathbf{q}/2 + \mathbf{p}'$ and $\mathbf{q}/2 - \mathbf{p}'$. Note that for particles in the single particle ground state, the z component of the momentum is zero. As we showed earlier, the ultraviolet divergences in the t-matrix can be renormalized in terms of cutoff-independent low energy parameters [19], and in the isotropic case, the t-matrix depends only on the spin-orbit coupling strength, the scattering lengths, and the incident and outgoing momenta. The exact summation of ladder diagrams for the t-matrix, for both isotropic and anisotropic spin-orbit couplings, is then (see Appendix A for the derivation):

$$\Gamma^{\alpha\alpha}_{\alpha\alpha}(\mathbf{p}, \mathbf{p}'; \mathbf{q}) = \frac{\pi}{m\kappa} \begin{pmatrix} 1 & e^{i(\phi_1+\phi_2)} & \dfrac{e^{i\phi_1} + e^{i\phi_2}}{2} \end{pmatrix} M^{-1} \begin{pmatrix} 1 \\ e^{-i(\phi_3+\phi_4)} \\ \dfrac{e^{-i\phi_3} + e^{-i\phi_4}}{2} \end{pmatrix}, \quad (8)$$

where

$$M = \begin{pmatrix} f(\frac{\tilde{q}}{2}) + \frac{1}{\kappa a_{aa}} & h_1(\tilde{\mathbf{q}}/2) & h_2(\tilde{\mathbf{q}}/2) \\ h_1^*(\tilde{\mathbf{q}}/2) & f(\frac{\tilde{q}}{2}) + \frac{1}{\kappa a_{bb}} & h_2^*(\tilde{\mathbf{q}}/2) \\ h_2^*(\tilde{\mathbf{q}}/2) & h_2(\tilde{\mathbf{q}}/2) & \frac{1}{2}\left(f(\frac{\tilde{q}}{2}) - g(\frac{\tilde{q}}{2}) + \frac{1}{\kappa a_{ab}}\right) \end{pmatrix}, \tag{9}$$

with $\bar{\mathbf{q}} \equiv \mathbf{q}/\kappa$ and $\tilde{q} \equiv q/\kappa$. The angles ϕ_1, ϕ_2, ϕ_3, and ϕ_4 are those of the vectors $\mathbf{q}/2+\mathbf{p}$, $\mathbf{q}/2-\mathbf{p}$, $\mathbf{q}/2-\mathbf{p}'$, and $\mathbf{q}/2+\mathbf{p}'$ in the x-y plane with a factor of η multiplying the y-components. The dimensionless functions $f(\tilde{q}/2)$, $g(\tilde{q}/2)$, $h_1(\tilde{\mathbf{q}}/2)$ and $h_2(\tilde{\mathbf{q}}/2)$ are,

$$\begin{aligned}
f(\tilde{q}/2) &\equiv \frac{\pi}{m\kappa}\int\frac{d^3k}{(2\pi)^3}\left[\frac{1}{\epsilon_-(\frac{\mathbf{q}}{2}+\mathbf{k})+\epsilon_-(\frac{\mathbf{q}}{2}-\mathbf{k})}+\right.\\
&\left.\frac{1}{\epsilon_+(\frac{\mathbf{q}}{2}+\mathbf{k})+\epsilon_+(\frac{\mathbf{q}}{2}-\mathbf{k})}+\frac{2}{\epsilon_-(\frac{\mathbf{q}}{2}+\mathbf{k})+\epsilon_+(\frac{\mathbf{q}}{2}-\mathbf{k})}-\frac{4m}{k^2}\right]\\
g(\tilde{q}/2) &\equiv -\frac{\pi}{m\kappa}\int\frac{d^3k}{(2\pi)^3}\left[\frac{\cos(\phi_5-\phi_6)}{\epsilon_-(\frac{\mathbf{q}}{2}+\mathbf{k})+\epsilon_-(\frac{\mathbf{q}}{2}-\mathbf{k})}\right.\\
&\left.+\frac{\cos(\phi_5-\phi_6)}{\epsilon_+(\frac{\mathbf{q}}{2}+\mathbf{k})+\epsilon_+(\frac{\mathbf{q}}{2}-\mathbf{k})}-\frac{2\cos(\phi_5-\phi_6)}{\epsilon_-(\frac{\mathbf{q}}{2}+\mathbf{k})+\epsilon_+(\frac{\mathbf{q}}{2}-\mathbf{k})}\right]\\
h_1(\tilde{\mathbf{q}}/2) &\equiv \frac{\pi}{m\kappa}\int\frac{d^3k}{(2\pi)^3}\left[\frac{e^{i(\phi_5+\phi_6)}}{\epsilon_-(\frac{\mathbf{q}}{2}+\mathbf{k})+\epsilon_-(\frac{\mathbf{q}}{2}-\mathbf{k})}\right.\\
&\left.+\frac{e^{i(\phi_5+\phi_6)}}{\epsilon_+(\frac{\mathbf{q}}{2}+\mathbf{k})+\epsilon_+(\frac{\mathbf{q}}{2}-\mathbf{k})}-\frac{2e^{i(\phi_5+\phi_6)}}{\epsilon_-(\frac{\mathbf{q}}{2}+\mathbf{k})+\epsilon_+(\frac{\mathbf{q}}{2}-\mathbf{k})}\right]\\
h_2(\tilde{\mathbf{q}}/2) &\equiv \frac{\pi}{2m\kappa}\int\frac{d^3k}{(2\pi)^3}\left[\frac{e^{i\phi_5}+e^{i\phi_6}}{\epsilon_-(\frac{\mathbf{q}}{2}+\mathbf{k})+\epsilon_-(\frac{\mathbf{q}}{2}-\mathbf{k})}\right.\\
&\left.-\frac{e^{i\phi_5}+e^{i\phi_6}}{\epsilon_+(\frac{\mathbf{q}}{2}+\mathbf{k})+\epsilon_+(\frac{\mathbf{q}}{2}-\mathbf{k})}-\frac{2(e^{i\phi_5}-e^{i\phi_6})}{\epsilon_-(\frac{\mathbf{q}}{2}+\mathbf{k})+\epsilon_+(\frac{\mathbf{q}}{2}-\mathbf{k})}\right],
\end{aligned} \tag{10}$$

where ϕ_5 and ϕ_6 are the angles of $\mathbf{q}/2-\mathbf{k}$ and $\mathbf{q}/2+\mathbf{k}$ in the x-y plane with y-components multiplied by η. Changing the angle of $\mathbf{q}$ in the x-y plane only changes the overall phases of $h_1(\tilde{\mathbf{q}}/2)$ and $h_2(\tilde{\mathbf{q}}/2)$. These four functions are everywhere finite except for the logarithmic divergence of $f(\tilde{q}/2)$ at $\tilde{q}=0$. When the scattering lengths are small, the diagonal elements of M are dominant and we may ignore the off-diagonal elements; the t-matrix thus obtained does not have terms containing products of different scattering lengths, the approximate result obtained for the bosonic t-matrix in [19].

IV. GROUND STATE PHASES

We now determine the many-body ground state via mean field theory using the t-matrix derived above as the effective interactions, an approximation valid as long as the na_{ij}^3 are all $\ll 1$, where n is the particle density. In mean field, we assume that all particles are in the single-particle ground states $(\kappa,0,0)$ or $(-\kappa,0,0)$, and thus ignore possible occupation of excited states as a consequence of the interaction. In this case the system is described essentially by the Nozières model [20]. The issues of going beyond mean field, e.g., via Bogoliubov theory, as well as including possible effects of the condensate on the effective interaction, are beyond the scope of this paper and are left for the future. For $0 \le \eta < 1$, we take the particles to be either at $\mathbf{p} = (\kappa,0,0)$ or $(-\kappa,0,0)$; the relevant interactions are those between particles of either the same momentum or opposite momenta. We denote the interaction with same momentum by $\Gamma_0 \equiv \Gamma^{\alpha\alpha}_{\alpha\alpha}(0,0;\pm 2\mathbf{K})$ and that with opposite momenta by $\Gamma_\pi \equiv \Gamma^{\alpha\alpha}_{\alpha\alpha}(\pm\mathbf{K},\mp\mathbf{K},0)$, where we use the abbreviated notation $\mathbf{K} \equiv (\kappa,0,0)$.

The relevant terms in the interaction are then equivalent to the Nozières model [20]

$$\mathcal{H}_{\rm int} \sim \frac{1}{2V}\Gamma_0 N(N+1) \ + \frac{1}{V}(2\Gamma_\pi - \Gamma_0)N_\pi N_0, \tag{11}$$

where $N_0 \equiv \alpha^\dagger_{(\kappa,0,0)}\alpha_{(\kappa,0,0)}$ and $N_\pi \equiv \alpha^\dagger_{(-\kappa,0,0)}\alpha_{(-\kappa,0,0)}$. The total number of particles, $N = N_0 + N_\pi$, is fixed. For $\Gamma_0 < 2\Gamma_\pi$, the ground state is a single BEC with either all the particles in $(\kappa,0,0)$ or $(-\kappa,0,0)$, while for $\Gamma_0 > 2\Gamma_\pi$, the condensate is nominally fragmented with half of atoms forming a BEC in one state and the other half forming a BEC in the other state. However, as shown in Ref. [23], such a fragmented state is expected to be unstable against formation of a coherent condensate with a condensate wave function that is a coherent superposition of the two momenta. Following the conventions of Refs. [14, 15], we call the single BEC phase "plane wave", and the BEC phase with two different momenta "striped." The difference of the present calculation from earlier studies with mean-field couplings [14, 15], is that here the bare couplings, $\mathcal{V}^{(1)}_{0,0;0,0}$ and $\mathcal{V}^{(1)}_{0,\pi;0,\pi}$, are replaced by Γ_0 and Γ_π respectively.

While there is no difficulty in deriving the phase diagrams for general scattering lengths, we assume here for simplicity that the intraspecies scattering lengths are equal, $a_{aa} = a_{bb}$. Then,

$$\begin{aligned}
\Gamma_0 &= \frac{2\pi}{m\kappa}\times\\
&\frac{1/\kappa a_{aa} + 1/\kappa a_{ab} + 2f(1) - g(1) + h_1(1) - 4h_2(1)}{(1/\kappa a_{ab} + f(1) - g(1))(1/\kappa a_{aa} + f(1) + h_1(1)) - 4h_2(1)^2}\\
\Gamma_\pi &= \frac{2\pi}{m\kappa}\frac{1}{1/\kappa a_{aa} + f(0) - h_1(0)},
\end{aligned} \tag{12}$$

where $h_1(0) \equiv h_1(\tilde{\mathbf{q}} = (0,0,0))$, $h_1(1) \equiv h_1(\tilde{\mathbf{q}} = (1,0,0))$, etc. The quantities $f(0), h_1(0), f(1), g(1), h_1(1)$, and $h_2(1)$, which depend on η, can be calculated numerically. The interaction between different momenta Γ_π is independent of a_{ab}, and is a monotonically increasing nonnegative function of κa_{aa}, equal to 0 at $\kappa a_{aa} = 0$ and reaching $2\pi/\left[m\kappa(f(0) - h_1(0))\right]$ at $\kappa a_{aa} = \infty$. The dependence of Γ_0 on κa_{aa} and κa_{ab} is more complicated. We plot

Γ_0 and Γ_π, both scaled by $2\pi/m\kappa$, for $\eta = 0.5$ in Fig. 1. Now we discuss the ground state phases from $\eta = 0$ to 1.

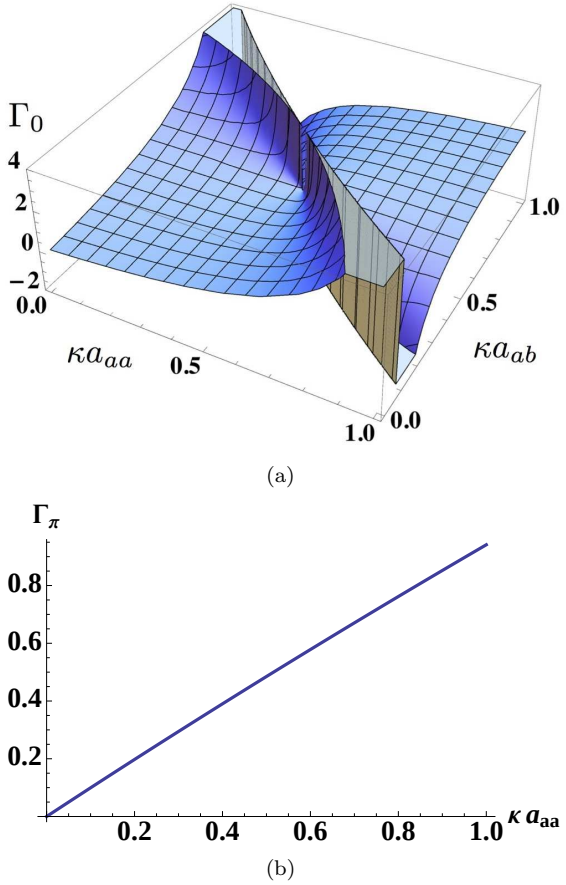

FIG. 1: (Color online) (a) Γ_0 as a function of κa_{aa} and κa_{ab}, and (b) Γ_π as a function of κa_{aa}, both scaled by $2\pi/m\kappa$, for $\eta = 0.5$. The vertical plane in the middle of panel (a) indicates the resonance where, from left to right, Γ_0 diverges to positive infinity and comes back from negative infinity.

When $\eta = 0$, the effective interactions are relatively simple. It can be shown that $f(0) = h_1(0)$ for $\eta = 0$; hence $\Gamma_\pi = 2\pi a_{aa}/m$, and the effective interaction in the $\mathbf{q} = 0$ channel does not depend on the spin-orbit coupling strength κ. In the $\mathbf{q}/2 = (\kappa, 0, 0)$ channel, $f(1) = -1, g(1) = 0, h_1(1) = 0$, and $h_2(1) = 1/2$, and thus,

$$\Gamma_0 = \frac{2\pi}{m\kappa} \frac{\kappa a_{aa} + \kappa a_{ab} - 4\kappa a_{aa} \cdot \kappa a_{ab}}{1 - \kappa a_{aa} - \kappa a_{ab}}$$

for $\eta = 0$. The effective interaction at small κa_{aa} and κa_{ab} is positive, and diverges when $\kappa a_{aa} + \kappa a_{ab}$ approaches unity. As one crosses the line $\kappa a_{aa} + \kappa a_{ab} = 1$, Γ_0 starts at negative infinity and remains negative until $\kappa a_{aa} + \kappa a_{ab} = 4\kappa a_{aa} \cdot \kappa a_{ab}$, after which Γ_0 is positive. When Γ_0 is negative, we expect the BEC in bulk to be unstable against collapse, as in ordinary BECs with negative scattering length in the absence of spin-orbit couplings. We call the phase with an attractive interaction "unstable." The three possible ground state phases, plane wave, striped, and unstable, are determined by the sign of Γ_0 and the interplay between Γ_0 and Γ_π.

As η increases from 0, the basic structure of Γ_0 does not change; Γ_0 remains positive at small κa_{aa} and κa_{ab}, and as these variables increase, Γ_0 again diverges at a line in the κa_{aa}-κa_{ab} plane, beyond which it is negative up to a second line, after which Γ_0 is positive. Since the denominator of Eq. (12) for Γ_0 is quadratic in the $1/\kappa a$, it has in fact two zeroes, the one for positive scattering lengths, as shown, and a second for negative scattering lengths, which is discussed at the end of this section. The structure for positive scattering lengths is illustrated in Fig. 1, for $\eta = 0.5$.

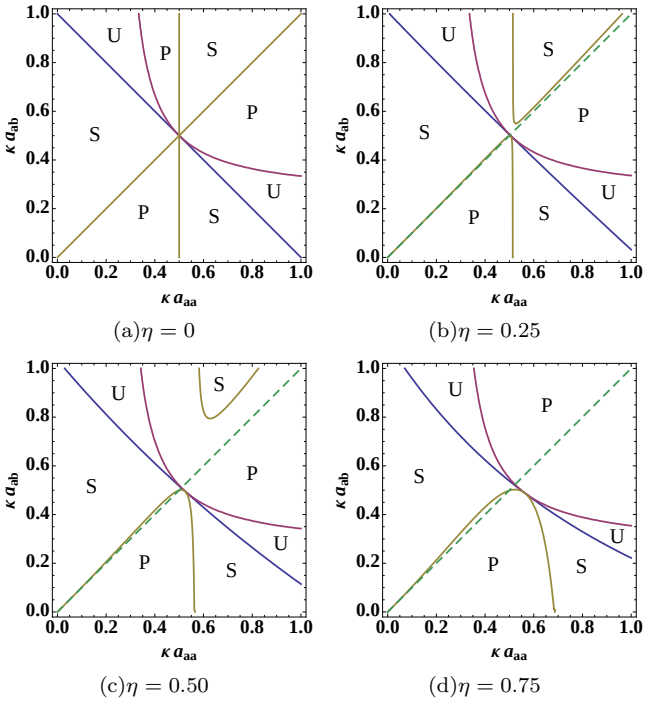

FIG. 2: (Color online) Ground state phase diagrams in the κa_{aa} - κa_{ab} plane for anisotropies $\eta = 0$, 0.25, 0.5, and 0.75. The regions P are the plane wave phase with a BEC of a single momentum. The regions S are the striped phase with a BEC of a coherent superposition of two different momenta. The phase in the regions U are unstable, with the effective interaction Γ_0 negative. Along the line between S and U, Γ_0 diverges, and along the line between U and P, Γ_0 vanishes. The intersection of these two lines is a critical point. The dashed lines indicate the phase diagram derived using mean-field coupling, in which the plane is separated into an upper striped region and a lower plane wave region.

The ground state phase diagrams for various η are plotted in Fig. 2. In the panels, the plane-wave phase is labelled "P," the striped phase "S," and the unstable phase "U." The plane-wave phase occurs when $\Gamma_0 < 2\Gamma_\pi$, the striped phase when $\Gamma_0 > 2\Gamma_\pi$, and the unstable phase when $\Gamma_0 < 0$. Note the overall tendency of the phase diagrams as η increases; the upper striped region detaches

from the resonant critical point, where the resonant line (between S and U) and the line with $\Gamma_0 = 0$ (between U and P) touch, and the region is pushed upwards as η is increased. Meanwhile, the shapes of the resonant line and the boundaries of plane wave regions change but, with the exception of the upper striped region the overall topology does not change. The dashed lines $a_{aa} = a_{ab}$ in the figures are the phase separation lines obtained earlier [14] using mean-field couplings $4\pi a_{aa}/m$ and $4\pi a_{ab}/m$; there the striped phase is preferred above and the plane wave phase below the dashed lines. Use of mean-field couplings is accurate for small κa_{aa} and κa_{ab}, but as these variables increase, the deviation from the mean-field coupling prediction becomes significant and the phase diagrams exhibit qualitatively new and rich structures.

This overall tendency continues to around $\eta \sim 0.99$. With further increase of η towards isotropy, $\eta = 1$, we start to observe qualitatively new behavior of the phase diagrams. The phase diagrams close to $\eta = 1$ are plotted in Fig. 3. As one sees, the striped region comes back from

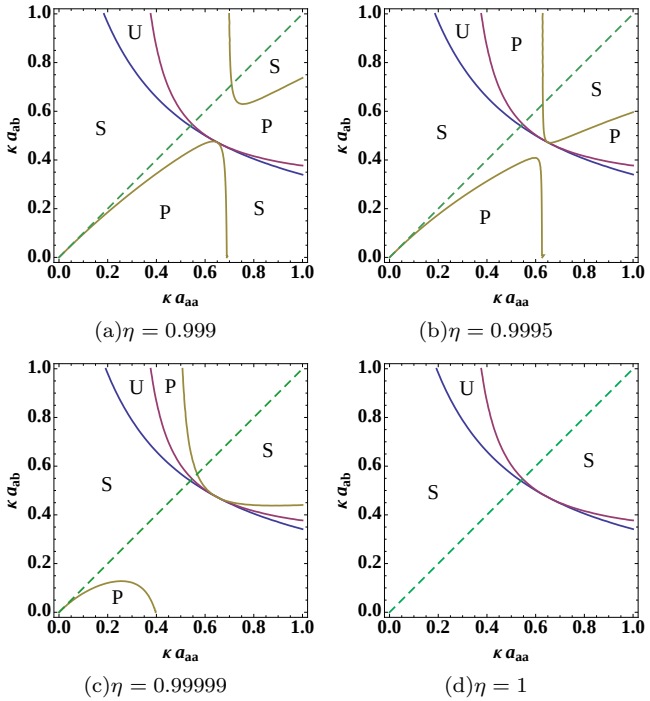

FIG. 3: (Color online) Ground state phase diagrams for η close to unity.

above and touches the resonant critical point, and at the same time the lower plane wave region detaches from the critical point. In the limit $\eta = 1$, the plane wave region vanishes.

The behavior around $\eta \simeq 1$ is in fact logarithmic in the deviations of the anisotropy η from unity. We write $\delta = 1 - \eta^2$; as $\delta \to 0$, $h_1(0)$, $f(1)$, $g(1)$, $h_1(1)$, and $h_2(1)$ approach finite values, but, in leading order for small δ, $f(0) \sim |\log\delta|/4$. Setting, for small δ, $h_1(0)$, $f(1)$, $g(1)$, $h_1(1)$, and $h_2(1)$ to their values at $\delta = 0$ and approximating $f(0)$ by $|\log\delta|/4$, corresponds to fixing Γ_0 and varying the slope of Γ_π. In the isotropic limit $\delta = 0$, $\Gamma_\pi = 0$ and thus a plane wave region is not allowed (cf. Eq. (11)). With small anisotropy, Γ_π can be positive, and small plane wave regions appear.

We briefly consider tuning the scattering lengths to negative values. In the absence of spin-orbit couplings, negative scattering lengths lead to an instability in large systems. On the other hand, as we see from Eq. (12), tuning the inverse scattering lengths to just below 0 does not immediately lead to an attractive interaction; in the presence of the spin-orbit coupling fields, Rashba-Dresselhaus couplings can stabilize BECs with negative scattering lengths if the inverse scattering lengths are small. Even when Γ_0 is negative, systems with small particle number can be metasble in the presence of an attractive interaction [26]. For illustration, we plot the phase diagram for $\eta = 0.5$ extended to negative scattering lengths in Fig. 4. In the regions marked "Stable," $\Gamma_0 > 0$ and the ground state is either a plane wave or striped phase. As seen in the figure, when both scattering lengths a_{aa} and a_{ab} are negative and large, another stable region appears in the phase diagram, in which the ground state is in the striped phase. The line between the lower left striped phase and the unstable phase is a second resonant line along which Γ_0 diverges. A stable region with negative scattering lengths generally exists for all $0 < \eta \leq 1$; as η increases, the stable region in the phase diagram becomes larger.

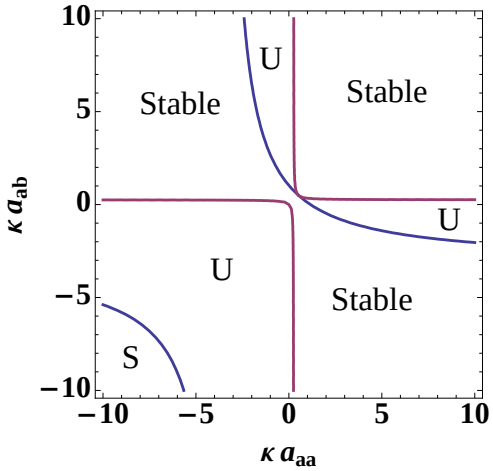

FIG. 4: (Color online) Ground state phase diagram for $\eta = 0.5$ extended to negative values of scattering lengths. The regions marked U and S are unstable and striped phases, as before. The region marked "Stable" is either a plane wave or striped phase. Note the appearance of a stable (striped) phase when both scattering lengths are large and negative.

V. CONCLUSION

Proposed schemes to realize Rashba-Dresselhaus spin-orbit couplings in ultracold atomic experiments [5–9] use Raman lasers to couple atoms in different hyperfine states. In general as one transforms the original basis to one in which the coupling has the Rashba-Dresselhaus spin-orbit structure, the interaction Hamiltonian acquires terms such as $a^\dagger_{\mathbf{p}_4} a^\dagger_{\mathbf{p}_3} a_{\mathbf{p}_2} b_{\mathbf{p}_1}$ which do not conserve the number of particles in each pseudospin state (a-like and b-like). Our analysis, which did not take such terms into account, can be directly compared with proposed experiments when the interaction is independent of species ($g_{aa} = g_{bb} = g_{ab}$), in which case the interaction is independent of the choice of basis. This condition is a good approximation for the three hyperfine states of ^{87}Rb in the lowest $F = 1$ state. The assumption that $g_{aa} = g_{bb} = g_{ab}$ corresponds to the (dashed) diagonal lines in Figs. 2 and 3. Figure 5 shows the phase diagram in the η-κa plane, where a is the assumed common scattering length.

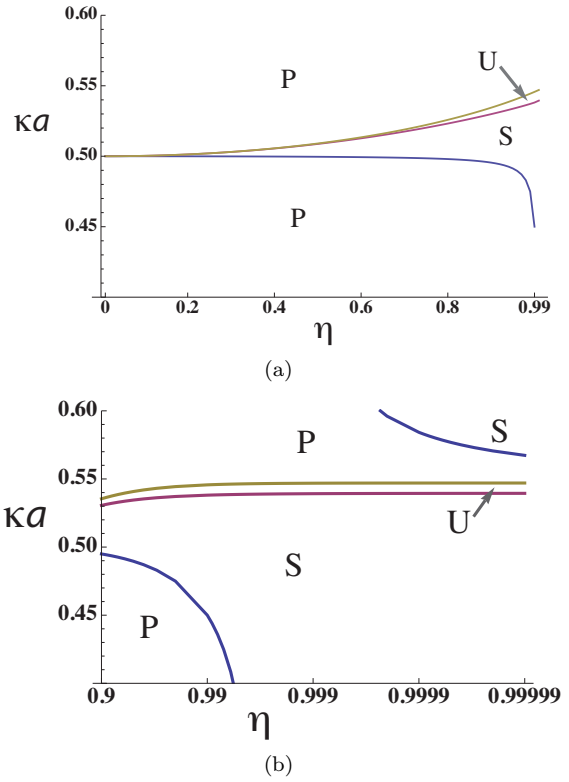

FIG. 5: (Color online) The ground state phase diagram when $a_{aa} = a_{bb} = a_{ab} = a$ in the η-κa plane for (a) anisotropies less than 0.99 and (b) anisotropies close to unity. The horizontal axis of panel (b) is a logarithmic scale.

For $0 \le \eta \le 0.99$ the system, with increasing κa, experiences transitions from plane wave to striped, then to unstable, and finally to the plane wave phase again as seen in Fig. 5(a). Looking more closely at the region $0.9 \le \eta \le 1$, as drawn on a logarithmic scale in Fig. 5(b), we find that the line separating the lower plane wave and striped region terminates and another line starts from positive infinity above which the striped phase is preferred. This new line touches the uppermost line (below the upper P phase) in the figure in the $\eta \to 1$ limit and thus no plane wave region exists at isotropic spin-orbit coupling [27].

Acknowledgments

We are extremely grateful to Professor Tin-Lun Ho for critical comments. This research was supported in part by NSF Grant PHY09-69790.

Appendix A: Exact summation of ladder diagrams for the t-matrix

Here we outline the derivation of the exact t-matrix (8). Our starting point is the set of Bethe-Salpeter equations:

$$\Gamma^{\alpha\alpha}_{\alpha\alpha}(\mathbf{p},\mathbf{p}';\mathbf{q}) = \mathcal{V}^{(1)}_{\phi_1,\phi_2;\phi_3,\phi_4} - \int \frac{d^3k}{(2\pi)^3}\left[\frac{\mathcal{V}^{(1)}_{\phi_1,\phi_2;\phi_5,\phi_6}\Gamma^{\alpha\alpha}_{\alpha\alpha}(\mathbf{k},\mathbf{p}';\mathbf{q})}{\epsilon_-(\frac{\mathbf{q}}{2}-\mathbf{k})+\epsilon_-(\frac{\mathbf{q}}{2}+\mathbf{k})} + \frac{\mathcal{V}^{(2)}_{\phi_1,\phi_2;\phi_5,\phi_6}\Gamma^{\alpha\alpha}_{\beta\beta}(\mathbf{k},\mathbf{p}';\mathbf{q})}{\epsilon_+(\frac{\mathbf{q}}{2}-\mathbf{k})+\epsilon_+(\frac{\mathbf{q}}{2}+\mathbf{k})} + \frac{\mathcal{V}^{(3)}_{\phi_1,\phi_2;\phi_6,\phi_5}\Gamma^{\alpha\alpha}_{\alpha\beta}(\mathbf{k},\mathbf{p}';\mathbf{q})}{\epsilon_+(\frac{\mathbf{q}}{2}-\mathbf{k})+\epsilon_-(\frac{\mathbf{q}}{2}+\mathbf{k})}\right]$$

$$\Gamma^{\alpha\alpha}_{\beta\beta}(\mathbf{p},\mathbf{p}';\mathbf{q}) = \mathcal{V}^{(2)}_{\phi_1,\phi_2;\phi_3,\phi_4} - \int \frac{d^3k}{(2\pi)^3}\left[\frac{\mathcal{V}^{(2)}_{\phi_1,\phi_2;\phi_5,\phi_6}\Gamma^{\alpha\alpha}_{\alpha\alpha}(\mathbf{k},\mathbf{p}';\mathbf{q})}{\epsilon_-(\frac{\mathbf{q}}{2}-\mathbf{k})+\epsilon_-(\frac{\mathbf{q}}{2}+\mathbf{k})} + \frac{\mathcal{V}^{(1)}_{\phi_1,\phi_2;\phi_5,\phi_6}\Gamma^{\alpha\alpha}_{\beta\beta}(\mathbf{k},\mathbf{p}';\mathbf{q})}{\epsilon_+(\frac{\mathbf{q}}{2}-\mathbf{k})+\epsilon_+(\frac{\mathbf{q}}{2}+\mathbf{k})} + \frac{\mathcal{V}^{(3)}_{\phi_1,\phi_2;\phi_5,\phi_6}\Gamma^{\alpha\alpha}_{\alpha\beta}(\mathbf{k},\mathbf{p}';\mathbf{q})}{\epsilon_+(\frac{\mathbf{q}}{2}-\mathbf{k})+\epsilon_-(\frac{\mathbf{q}}{2}+\mathbf{k})}\right]$$

and

$$\Gamma^{\alpha\alpha}_{\alpha\beta}(\mathbf{p},\mathbf{p}';\mathbf{q}) = \mathcal{V}^{(4)}_{\phi_1,\phi_2;\phi_3,\phi_4} - \int \frac{d^3k}{(2\pi)^3}\left[\frac{\mathcal{V}^{(4)}_{\phi_1,\phi_2;\phi_5,\phi_6}\Gamma^{\alpha\alpha}_{\alpha\alpha}(\mathbf{k},\mathbf{p}';\mathbf{q})}{\epsilon_-(\frac{\mathbf{q}}{2}-\mathbf{k})+\epsilon_-(\frac{\mathbf{q}}{2}+\mathbf{k})} + \frac{\mathcal{V}^{(4)}_{\phi_2,\phi_1;\phi_5,\phi_6}\Gamma^{\alpha\alpha}_{\beta\beta}(\mathbf{k},\mathbf{p}';\mathbf{q})}{\epsilon_+(\frac{\mathbf{q}}{2}-\mathbf{k})+\epsilon_+(\frac{\mathbf{q}}{2}+\mathbf{k})} + \frac{\mathcal{V}^{(5)}_{\phi_1,\phi_2;\phi_6,\phi_5}\Gamma^{\alpha\alpha}_{\alpha\beta}(\mathbf{k},\mathbf{p}';\mathbf{q})}{\epsilon_+(\frac{\mathbf{q}}{2}-\mathbf{k})+\epsilon_-(\frac{\mathbf{q}}{2}+\mathbf{k})}\right], \tag{A1}$$

where $\Gamma^{\rho\tau}_{\mu\nu}(\mathbf{p},\mathbf{p}';\mathbf{q})$ is the t-matrix for scattering of particles in the branches μ,ν with momenta $\mathbf{q}/2 \pm \mathbf{p}$ to branches ρ,τ with final momenta $\mathbf{q}/2 \pm \mathbf{p}'$. The key to solving this set of equations is to construct the quan-

tities

$$X(\mathbf{p},\mathbf{p}';\mathbf{q}) \equiv \frac{1}{4}\left(\Gamma^{\alpha\alpha}_{\alpha\alpha}(\mathbf{p},\mathbf{p}';\mathbf{q}) + \Gamma^{\alpha\alpha}_{\beta\beta}(\mathbf{p},\mathbf{p}';\mathbf{q}) + \Gamma^{\alpha\alpha}_{\alpha\beta}(\mathbf{p},\mathbf{p}';\mathbf{q})/\sqrt{2} + \Gamma^{\alpha\alpha}_{\alpha\beta}(-\mathbf{p},\mathbf{p}';\mathbf{q})/\sqrt{2}\right),$$

$$Y(\mathbf{p},\mathbf{p}';\mathbf{q})e^{-i(\phi_3+\phi_4)} \equiv \frac{1}{4}\left(\Gamma^{\alpha\alpha}_{\alpha\alpha}(\mathbf{p},\mathbf{p}';\mathbf{q}) + \Gamma^{\alpha\alpha}_{\beta\beta}(\mathbf{p},\mathbf{p}';\mathbf{q}) - \Gamma^{\alpha\alpha}_{\alpha\beta}(\mathbf{p},\mathbf{p}';\mathbf{q})/\sqrt{2} - \Gamma^{\alpha\alpha}_{\alpha\beta}(-\mathbf{p},\mathbf{p}';\mathbf{q})/\sqrt{2}\right) e^{-i(\phi_1+\phi_2)},$$

and

$$Z(\mathbf{p},\mathbf{p}';\mathbf{q}) \equiv \frac{1}{2}\frac{\Gamma^{\alpha\alpha}_{\alpha\alpha}(\mathbf{p},\mathbf{p}';\mathbf{q}) - \Gamma^{\beta\beta}_{\alpha\alpha}(\mathbf{p},\mathbf{p}';\mathbf{q})}{(e^{i\phi_1}+e^{i\phi_2})(e^{-i\phi_3}+e^{-i\phi_4})} = \frac{1}{2}\frac{\Gamma^{\alpha\alpha}_{\alpha\beta}(\mathbf{p},\mathbf{p}';\mathbf{q})/\sqrt{2} - \Gamma^{\alpha\alpha}_{\alpha\beta}(-\mathbf{p},\mathbf{p}';\mathbf{q})/\sqrt{2}}{(e^{i\phi_1}-e^{i\phi_2})(e^{-i\phi_3}+e^{-i\phi_4})}. \quad \text{(A2)}$$

Rewriting the Bethe-Salpeter equations in terms of X, Y, and Z, we see that X, Y, and Z do not depend on their first arguments. Namely, we can write $X(\mathbf{p},\mathbf{p}';\mathbf{q}) = X(\mathbf{p}';\mathbf{q})$, etc. Then X, Y, and Z inside the integrals can be moved outside, and we can solve for X, Y, and Z algebraically, and reconstruct $\Gamma^{\alpha\alpha}_{\alpha\alpha}$ from X, Y, and Z via

$$\Gamma^{\alpha\alpha}_{\alpha\alpha}(\mathbf{p},\mathbf{p}';\mathbf{q}) = X(\mathbf{p}';\mathbf{q}) + Y(\mathbf{p}';\mathbf{q})e^{i(\phi_1+\phi_2-\phi_3-\phi_4)} + Z(\mathbf{p}';\mathbf{q})(e^{i\phi_1}+e^{i\phi_2})(e^{-i\phi_3}-e^{-i\phi_4}). \quad \text{(A3)}$$

Introducing the free field scattering lengths by $m/4\pi a_{ij} = 1/g_{ij} + m\Lambda/2\pi^2$, where Λ is the high momentum cutoff, we obtain Eq. (8).

[1] M. Hasan and C. Kane, Rev. Mod Phys. **82**, 3045 (2010).
[2] I. Žutić, J. Fabian, and S. Das Sarma, Rev. Mod. Phys. **76**, 323 (2004).
[3] J. Dalibard, F. Gerbier, G. Juzeliūnas, and P. Öhberg, arXiv:1008.5378.
[4] Y.-J. Lin, K. Jiménez-García, and I. B. Spielman, Nature **471**, 83 (2011).
[5] J. Ruseckas, G. Juzeliūnas, P. Öhberg, and M. Fleischhauer, Phys. Rev. Lett. **95**, 010404 (2005).
[6] S.-L. Zhu, H. Fu, C.-J. Wu, S.-C. Zhang, and L.-M. Duan, Phys. Rev. Lett. **97**, 240401 (2006).
[7] X.-J. Liu, M. F. Borunda, X. Liu, and J. Sinova, Phys. Rev. Lett. **102**, 046402 (2009).
[8] G. Juzeliūnas, J. Ruseckas, and J. Dalibard, Phys. Rev. A **81**, 053403 (2010).
[9] D. L. Campbell, G. Juzeliūnas, and I. B. Spielman, arXiv:1102.3945.
[10] E. I. Rashba, Fiz. Tverd. Tela, **2**, 1224 (1960) [Sov. Phys. Solid State **2**, 1109 (1960)].
[11] G. Dresselhaus, Phys. Rev. **100**, 580–586 (1955).
[12] T. D. Stanescu, B. Anderson, and V. Galitski, Phys. Rev. A **78**, 023616 (2008).
[13] C. Wu, I. Mondragon-Shem, and X.-F. Zhou, Chin. Phys. Lett. **28**, 097102 (2011).
[14] C. Wang, C. Gao, C.-M. Jian, and H. Zhai, Phys. Rev. Lett. **105**, 160403 (2010).
[15] C.-M. Jian and H. Zhai, Phys. Rev. B **84**, 060508(R) (2011).
[16] S.-K. Yip, Phys. Rev. A **83**, 043616 (2011).
[17] Y. Zhang, L. Mao, and C. Zhang, arXiv:1102.4045.
[18] S. Gopalakrishnan, A. Lamacraft, and P. M. Goldbart, arXiv:1106.2552.
[19] T. Ozawa and G. Baym, arXiv:1107.3162.
[20] P. Nozières, in *Bose-Einstein Condensation*, A. Griffin, D. W. Snoke, and S. Stringari, eds. (Cambridge Univ. Press, Cambridge, 1995).
[21] T.-L. Ho and V. B. Shenoy , Phys. Rev. Lett. **77**, 3276 (1996).
[22] T.-L. Ho and S. Zhang, arXiv:1007.0650, PRL in press.
[23] E. J. Mueller, T.-L. Ho, M. Ueda, and G. Baym, Phys. Rev. A **74**, 033612 (2006).
[24] G. Baym and C. J. Pethick, Phys. Rev. Lett. **76**, 6 (1996).
[25] That there are only three possible phases is, as pointed out in Ref. [21], a consequence of the system having just two pseudospin components, which when dressed by a spin-orbit interaction can be miscible (the striped phase), immiscible (the plane wave phase), or unstable. See Ref. [22] for a discussion of the experiment of Ref. [4].
[26] Assuming bosons trapped in an isotropic harmonic potential, we can roughly estimate the particle number below which the condensate is stable with $\Gamma_0 < 0$. In the absence of spin-orbit coupling, the critical number of bosons is $N_c \sim 0.6a_{\rm osc}/|a|$, where $a_{\rm osc}$ is the oscillator length of a trap $\sqrt{\hbar/m\omega}$ [24]. For spin-orbit coupled bosons, the scattering length is replaced by $m\Gamma_0/4\pi$. Introducing a scaled effective coupling $\tilde{\Gamma}_0 = m\kappa\Gamma_0/2\pi$ (the scale used in Fig. 1), we estimate a critical number $N_c \sim 0.3\kappa a_{\rm osc}/|\tilde{\Gamma}_0|$. Using realistic values of $\kappa \sim \sqrt{2}\pi/804$nm [4] and $a_{\rm osc} \sim 1\mu$m, we obtain $N_c \sim 2/|\tilde{\Gamma}_0|$, which implies that stabilization occurs only quite close to the line $\Gamma_0 = 0$.
[27] While one can achieve large scattering lengths experimentally with Feshbach resonances, the general $m_F, m_{F'}$ dependence of the resonances leads to differences of the scattering lengths near the resonances, a complicating feature requiring analysis beyond the scope of this paper.